Article

Optomechanical dissipative solitons

https://doi.org/10.1038/s41586-021-04012-1

Received: 8 January 2020

Accepted: 9 September 2021

Published online: 1 December 2021

Check for updates

Jing Zhang[1,2], Bo Peng[1], Seunghwi Kim[3], Faraz Monifi[1], Xuefeng Jiang[1], Yihang Li[1], Peng Yu[4], Lianqing Liu[4], Yu-xi Liu[5], Andrea Alù[3,6] & Lan Yang[1]✉

Nonlinear wave–matter interactions may give rise to solitons, phenomena that feature inherent stability in wave propagation and unusual spectral characteristics. Solitons have been created in a variety of physical systems and have had important roles in a broad range of applications, including communications, spectroscopy and metrology[1–4]. In recent years, the realization of dissipative Kerr optical solitons in microcavities has led to the generation of frequency combs in a chip-scale platform[5–10]. Within a cavity, photons can interact with mechanical modes. Cavity optomechanics has found applications for frequency conversion, such as microwave-to-optical or radio-frequency-to-optical[11–13], of interest for communications and interfacing quantum systems operating at different frequencies. Here we report the observation of mechanical micro-solitons excited by optical fields in an optomechanical microresonator, expanding soliton generation in optical resonators to a different spectral window. The optical field circulating along the circumference of a whispering gallery mode resonator triggers a mechanical nonlinearity through optomechanical coupling, which in turn induces a time-varying periodic modulation on the propagating mechanical mode, leading to a tailored modal dispersion. Stable localized mechanical wave packets—mechanical solitons—can be realized when the mechanical loss is compensated by phonon gain and the optomechanical nonlinearity is balanced by the tailored modal dispersion. The realization of mechanical micro-solitons driven by light opens up new avenues for optomechanical technologies[14] and may find applications in acoustic sensing, information processing, energy storage, communications and surface acoustic wave technology.

Cavity optomechanics has attracted extensive attention in recent years, creating opportunities for high-precision sensing, communications and quantum information processing[14], as well as for fundamental science, for example, macroscopic quantum effects in mechanical systems[15] and gravitational wave detection[16]. Although most of the studies about cavity optomechanics focus on the 'cooling' regime—where the cavity is driven by a laser red-detuned from the cavity resonance and thus absorbs phonons from mechanical modes—extensive research has been recently devoted to the 'heating' regime of cavity optomechanics. In this regime, a photon blue-detuned from the cavity resonance will emit a phonon into the mechanical modes when entering the cavity. Various phenomena have been observed in this regime, such as phonon lasing, in which coherent mechanical vibrations are excited through optical pumping[17–19]. For strong pumps, it is also possible to observe nonlinear optical effects, such as chaos[20,21] optical solitons[22–24], and surface acoustic wave frequency combs[25–28].

Recently, optical solitons have been demonstrated and exploited in Kerr optical frequency combs, which provide robust, equally spaced spectral lines, ideally suited for timing and metrology[1–4]. These developments have enabled the realization of chip-scale frequency combs through Kerr nonlinearity or electro-optical interactions[29–32] obtained by balancing nonlinearity and dispersion in Kerr microresonators[5,33]. The phononic counterparts of the optical frequency comb, that is, mechanical frequency combs, have been theoretically proposed using Fermi–Pasta–Ulam–Tsingou chains, and later demonstrated in micromechanical resonators using nonlinear three-wave mixing[25,34,35]. Their repetition rates are from a few Hz up to kHz, ten orders of magnitude smaller than the typical rates of optical combs, implying much finer frequency resolution.

Here we investigate nonlinear mechanical phenomena in optomechanical resonators and report observation of mechanical micro-solitons in an optical whispering gallery mode (WGM) toroidal microresonator. Although optical solitons have been observed in various WGM microresonators[6–10], here we experimentally demonstrate optomechanical solitons—that is, localized acoustic waves stimulated by an optical pumping field—in WGM optomechanical resonators. In certain parameter regimes, we also observe mechanical frequency combs. The observed localized acoustic waves through optomechanical interactions are distinct from optical solitons—that is, localized photonic wavepackets, theoretically predicted in optomechanical arrays[22], in which both Kuznetsov–Ma solitons[23] and Akhmediev breathers[24] have been studied. In addition—unlike previous studies on frequency combs in optomechanical resonators[25–28] formed by cascaded four-wave

[1]Department of Electrical and Systems Engineering, Washington University, St. Louis, MO, USA. [2]Department of Automation, Tsinghua University, Beijing, P. R. China. [3]Photonics Initiative, Advanced Science Research Center, City University of New York, New York, NY, USA. [4]State Key Laboratory of Robotics, Shenyang Institute of Automation, Chinese Academy of Sciences, Shenyang, P. R. China. [5]Institute of Microelectronics, Tsinghua University, Beijing, P. R. China. [6]Physics Program, Graduate Center, City University of New York, New York, NY, USA. ✉e-mail: yang@seas.wustl.edu

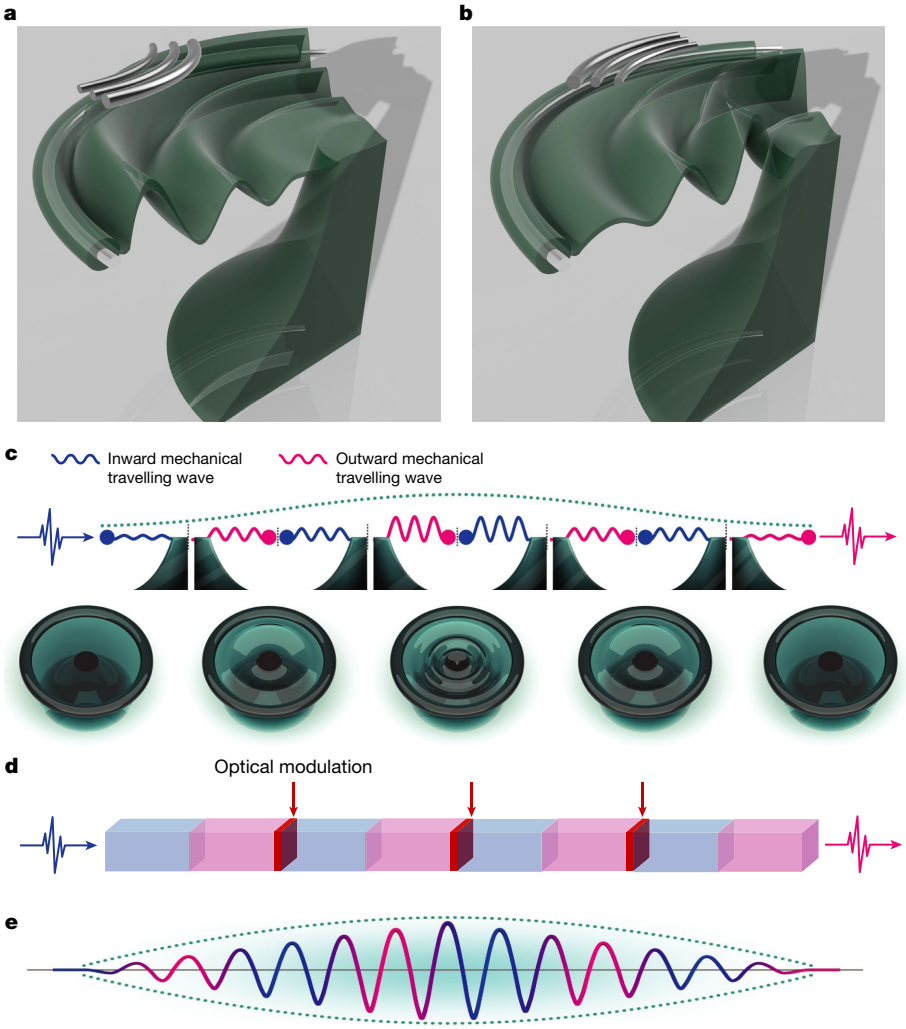

Fig. 1 | Mechanism of acoustic-wave propagation in an optomechanical resonator. a, An inward mechanical travelling wave is excited and periodically modulated by the optical field at the rim of the microresonator. **b**, An outward mechanical travelling wave reflected by the silicon pedestal. **c**, The multiple reflections, properly tailored by nonlinearities and modal dispersion, can form an optomechanical soliton with dimension much larger than the physical size of the resonator. Snapshots of the propagating mechanical travelling wave are shown as a function of time. **d**, An equivalent optomechanical lattice, in which the optical field modulates the mechanical travelling wave periodically. **e**, Analogy of the optomechanical micro-soliton to a conventional mechanical soliton. The blue and pink curves denote inward and reflected outward waves, respectively.

mixing of different mechanical modes via nonlinear optomechanical coupling—the frequency combs observed in our experiments stem from the cnoidal wave mechanical motion associated with soliton formation. As the pump grows, this periodic-pulse-type motion becomes localized and turns into a single mechanical wavepacket, supporting a mechanical micro-soliton.

Figure 1 shows a toroidal microdisk resonator supporting both high-quality factor (Q) optical and mechanical modes. We focus on radial mechanical modes supported by the thin disk (Fig. 1a–c). When a blue-detuned optical pump is coupled into the resonator, radial mechanical waves are excited. At the rim of the microresonator, the back-action of the optical mode leads to the indirect coupling between the counterpropagating mechanical modes. A high optical pump power triggers the nonlinearity in the mechanical wave propagating from the rim of the resonator towards the central pedestal (Fig. 1a). At the silicon pedestal, the mechanical travelling wave experiences a π phase shift upon reflection and travels back towards the perimeter of the toroid (Fig. 1b). Once the mechanical travelling wave meets the ring of the toroid where the optical mode resides, the optomechanical coupling enables optically induced modulation of the mechanical wave, which travels back towards the central pedestal again.

This multiple scattering process of the mechanical wave can be modelled as the propagation through an effective mechanical lattice[36] (Fig. 1d). Inward propagation towards the pedestal (illustrated by the blue travelling waves in Fig. 1c) experiences effective mechanical properties (blue block in Fig. 1d) that are different to those of outward travelling waves (red in Fig. 1c, d), owing to the different roles played by the nonlinear optomechanical interactions. Hence, the overall mechanical response of the toroid can be described by the effective mechanical lattice sketched in Fig. 1d, with an added π phase shift at the end of each red block (red arrows in Fig. 1d). This acoustic-wave lattice induces an unusual dispersion of the mechanical travelling wave. A self-reinforcing wavepacket (that is, a micro-soliton), following the same dynamics of a shallow-water wave with a weak nonlinear restoring force[37] (longwave scenario), can, therefore, arise in such a mechanical effective lattice. Figure 1e illustrates how the mechanical travelling waves collectively behave as a single wavepacket under the nonlinear coupling via optomechanical interactions with the blue-detuned pumping. The envelope of the mechanical wavepacket (see the green envelope in Fig. 1c and the wavepacket in Fig. 1e) is much larger than the unit cell of the mechanical lattice, and so the micro-soliton has a time-varying wave amplitude rather than a visualized packet in a single cell, as shown in Fig. 1c, d.

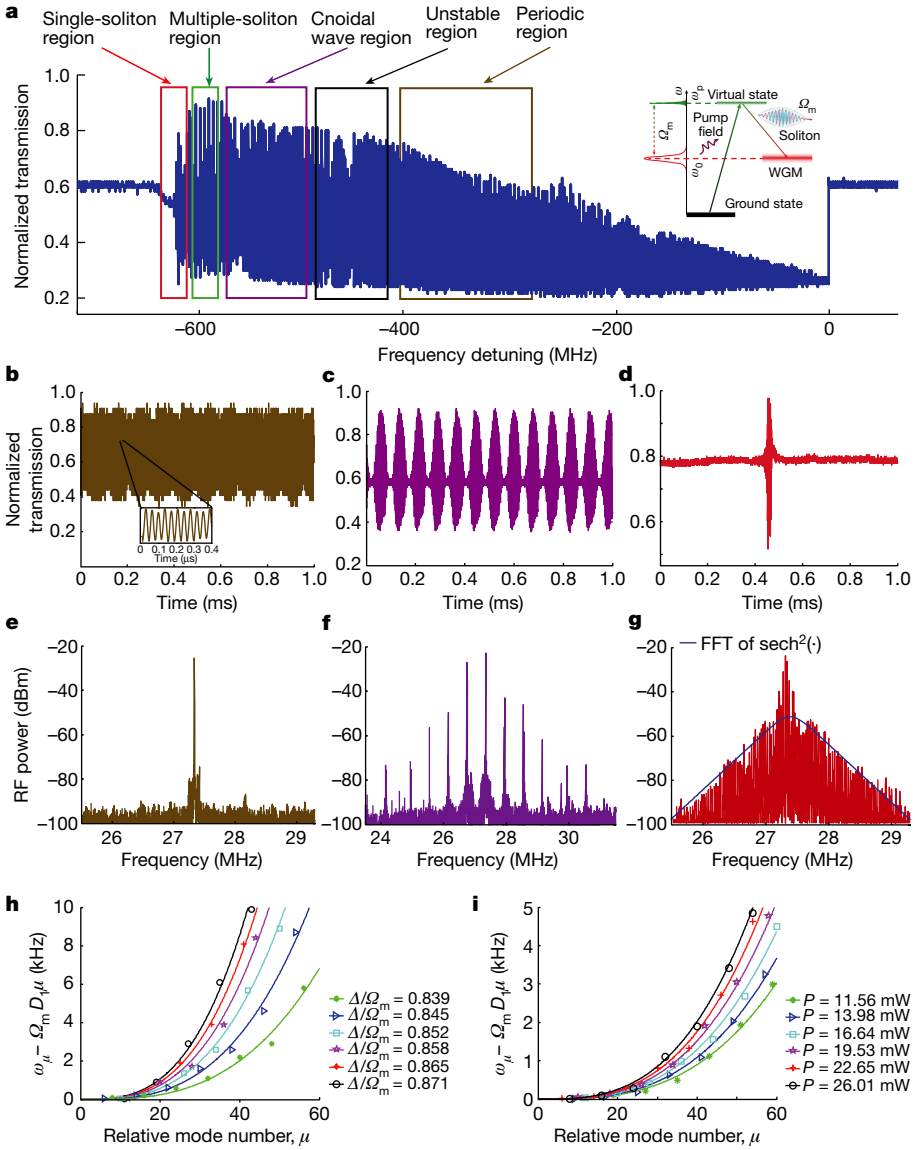

Fig. 2 | Generation of an optomechanical soliton. a, Different observed regimes as a function of frequency detuning between pump and cavity mode. Inset, the energy transfer mechanism from optical to mechanical mode. More energy can be efficiently fed into the mechanical mode from the optical mode under the matching condition $\Delta = \omega_p - \omega_0 = \Omega_m$, leading to the formation of mechanical solitons. ω_p, ω_0 and Δ are the frequencies of the pump field, cavity mode and frequency detuning, respectively, and Ω_m is the mechanical mode frequency. **b**–**d**, Time-domain spectra of the output field in periodic (**b**), cnoidal wave (**c**) and soliton (**d**) regimes. The frequency detuning of the input field increases from left to right, and we can observe phonon localization for increased frequency detuning. **e**–**g**, Output spectra in the frequency domain of the pump field in periodic (**e**; single peak), cnoidal wave (**f**; frequency-comb-type spectrum) and soliton (**g**; broadband peak) regimes. **h**, Dispersion spectra for different normalized frequency detunings. **i**, Dispersion spectra for different pump powers, *P*. dBm, decibel milliwatts; FFT, fast Fourier transform; RF, radio frequency; WGM, whispering gallery mode.

In the parameter space, the mechanical dynamics can experience different regimes. By tuning the pump power or the frequency detuning between the pump field and the cavity mode, transitions from sinusoidal to cnoidal and solitary regimes can be observed for the mechanical motion. When the optical pump power is low, the optomechanically induced mechanical nonlinearity can be neglected. A simple continuous sinusoidal wave is excited in the resonator. As the pump power increases, the system becomes unstable: the optomechanical interaction introduces a third-order mechanical nonlinear term[36]. Meanwhile, the optomechanical interaction modifies the dispersion relation as $\omega_\mu = \Omega_m + D_1\mu + D_3\mu^3$, where μ, D_1 and D_3 are the relative mode number and the first- and third-order dispersion coefficients of the mechanical travelling wave[36], respectively. The mechanical dispersion broadens the travelling wave, and the mechanical nonlinearity sharpens the wavepacket.

When nonlinearity and dispersion balance each other, a stable and localized mechanical wave packet, that is, an optomechanical soliton, is achieved. In the soliton regime, the shape of the soliton pulse can largely vary with pump power as well as with frequency detuning, which affects the strength of nonlinearity and the mode dispersion. This mechanism is quite different from the formation of optical solitons in microresonators described by the Lugiato–Lefever equation[5]. The dynamics of our soliton system can be characterized by the following modified Korteweg–de Vries equation,

$$\frac{\partial u}{\partial t} = [(G - \Gamma_m) - \xi u^2]u - v\frac{\partial u}{\partial z} - \sigma u\frac{\partial u}{\partial z} - d_{KdV}\frac{\partial^3 u}{\partial z^3} + \zeta(t), \quad (1)$$

where $u(z, t)$ is the amplitude of the mechanical travelling wave, z is the coordinate along the radius of the microtoroid, v is the effective

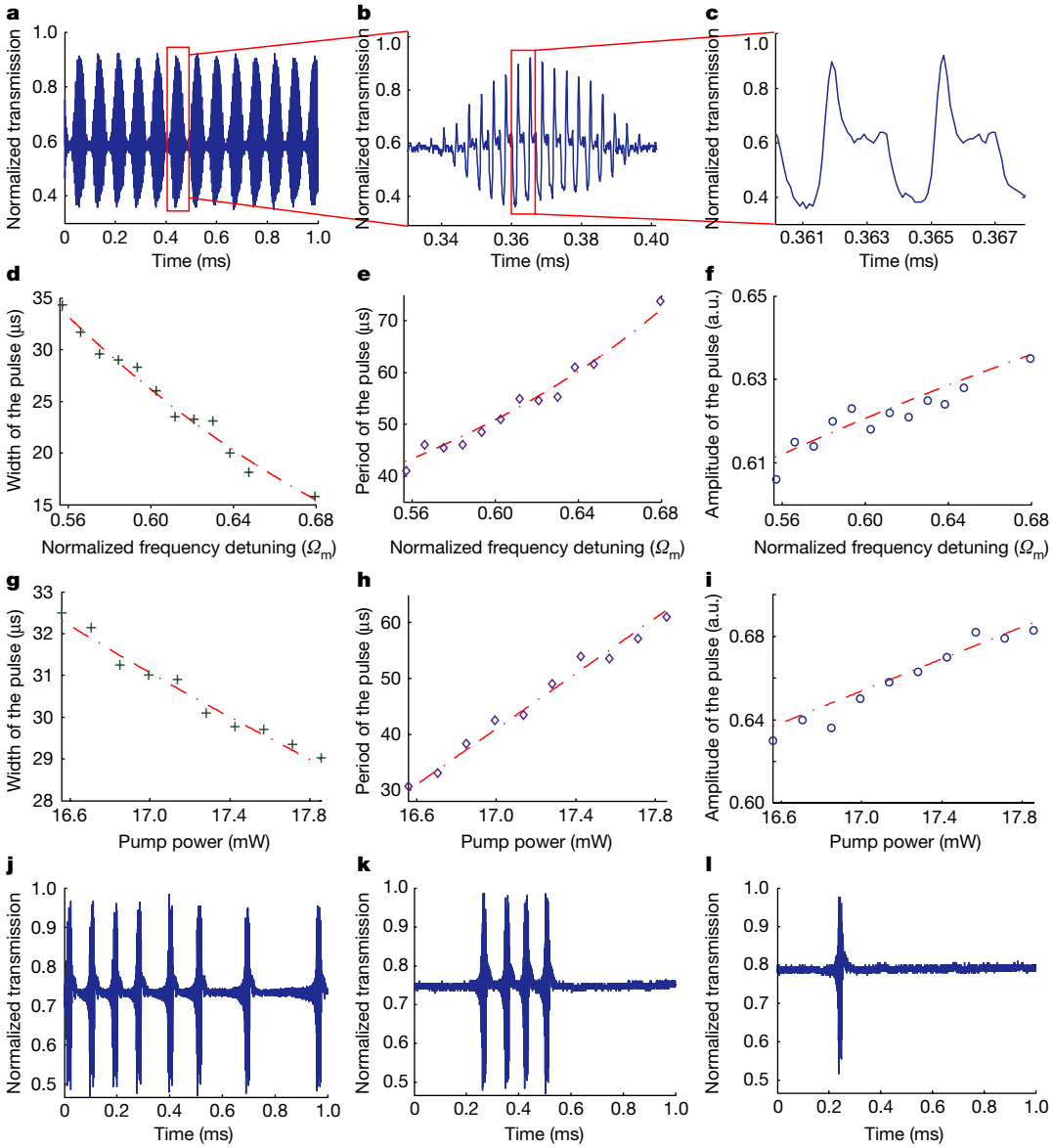

Fig. 3 | Localized periodic phonon pulses in the cnoidal wave regime and soliton regime. a–**c**, Slowly varying envelope of the amplitude of the periodic mechanical motion in the cnoidal wave regime with increasing magnification. **d**–**f**, Width (**d**), period (**e**) and amplitude (**f**) of the periodic pulses in the output field versus different frequency detunings of the input field in the cnoidal wave regime. **g**–**i**, Width (**g**), period (**h**) and amplitude (**i**) of the periodic pulses in the output field versus different input pump power in the cnoidal wave regime. The pulse width decreases, and period and amplitude increase with increased frequency detuning and pump power in the cnoidal wave regime. **j**–**l**, With increased detuning frequency, an eight-soliton pulse (**j**), a four-soliton pulse (**k**) and a single-soliton pulse (**l**) are generated. a.u., arbitrary units.

propagating speed of the soliton, σ is the aforementioned optomechanically induced third-order mechanical nonlinear coefficient, $d_{KdV} = (8\pi^3/\lambda^3)/D_3$ is the normalized third-order dispersion coefficient of the mechanical travelling wave, λ is the wavelength of the mechanical mode, G designates the mechanical gain induced by the phonon lasing effects, Γ_m characterizes the damping rate of the mechanical wave, ξ is the strength of the third-order mechanical nonlinear term induced by optomechanics, $\zeta(t)$ denotes white noise satisfying $E(\zeta(t)) = 0$, $E(\zeta(t)\zeta(t')) = D\delta(t - t')$ where $\delta(\cdot)$ is the Dirac delta function, which is 0 everywhere except at the origin, and its integral from $-\infty$ to $+\infty$ is equal to 1, and D is the strength of the noise. Note that the Korteweg–de Vries equation has been used to study mechanical solitons in shallow-water waves[37] as well as acoustic solitons in solid-state structures[36]. Unlike cavity optical solitons described by the Lugiato–Lefever equation, in which loss is compensated by a coherent input field[38–42], the mechanical loss in our system is compensated by mechanical gain and nonlinear saturation induced by phonon lasing. This is analogous to dissipative solitons observed in laser systems, in which loss is balanced by laser gain[43].

We experimentally observe these phenomena in an optomechanical microresonator with $\Omega_m = 27.3$ MHz and quality factor of 8×10^6 coupled to a tapered fibre. Several phase transitions of the mechanical mode can be observed by gradually increasing the blue detuning of the driving field from the resonant frequency (Fig. 2a). On the blue-detuned side, the energy is fed into the mechanical mode by the energy transfer between the optical pump and the cavity mode, as shown in the energy diagram in Fig. 2a, inset. When the detuning is much smaller than the mechanical frequency, a sinusoidal waveform is excited owing to a weak modulation of the mechanical mode by the optomechanical effects (Fig. 2b, e, which shows the temporal and frequency responses, respectively). A further increase of the detuning induces cascaded sidebands around the main peak of the mechanical mode in the frequency

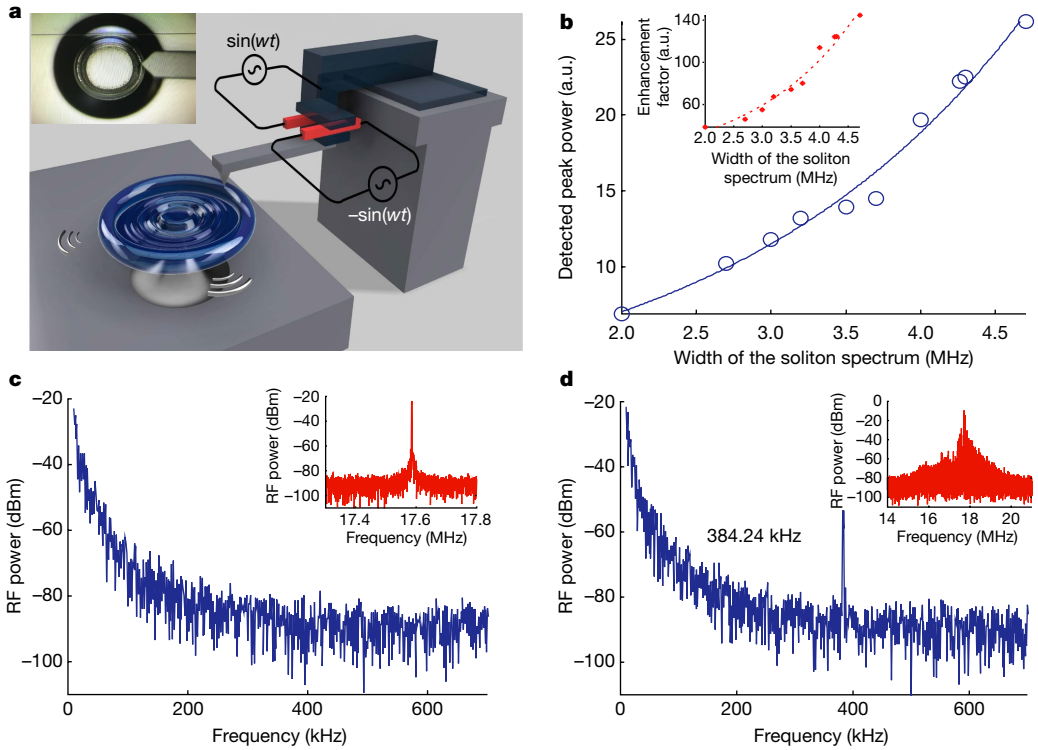

Fig. 4 | Detection of a low-frequency vibration of a cantilever tip by an optomechanical soliton. a, Schematic diagram of the experimental set-up. Inset, top view of the microtoroid and cantilever tip. **b**, Peak power of the spectrum for detecting the motion of the cantilever tip versus the width of the mechanical soliton in the frequency domain. Inset, the enhancement factor η versus the width of the mechanical soliton in the frequency domain. With the increase of the width of the mechanical soliton in the frequency domain, the cavity becomes more sensitive to the motion of the cantilever tip, owing to the increase of the enhancement factor η_{enh}. **c**, Power spectrum for detecting the mechanical motion of the cantilever tip when the mechanical mode of the microtoroid is in the periodic regime, in which the mechanical motion of the cantilever tip with eigenfrequency Ω_{tip} = 384.24 kHz (far off resonance from the eigenfrequency Ω_m (in MHz) of the mechanical mode of the microtoroid) cannot be detected. Inset, power spectrum of the mechanical mode of the microtoroid in the periodic regime. **d**, Power spectrum for detecting the mechanical motion of the cantilever tip when the mechanical mode of the microtoroid is in the soliton regime, in which the mechanical motion of the cantilever tip is observed. Inset, power spectrum of the microtoroid in the mechanical soliton regime. a.u., arbitrary units.

domain (Fig. 2f) and a periodic localized wavepacket in the time domain (Fig. 2c). The localized wavepacket observed here is induced by a particular mechanical motion of the microtoroid, cnoidal wave motion[44–46], which leads to a localized wavepacket in the output field. Further blue detuning towards the mechanical frequency leads to an increase in the period of the localized pulse, until the system enters a regime in which the recurrence of the localized pulse stops being periodic, and several localized pulses may appear at the same time. This corresponds to the multi-soliton regime, in which the mechanical nonlinearity is so strong that the localized mechanical wavepackets may not be stable, but they interact, merge and collide with each other. Finally, the single-soliton wavepacket regime is reached, when the blue detuning is close to the mechanical frequency. Under this condition, the mechanical mode is resonant with the radiation force; thus, energy can be efficiently transferred from the optical mode to the mechanical mode (Fig. 2a, inset), maximizing the optomechanically induced mechanical nonlinearity. In this regime, we can obtain maximum localization of the mechanical wavepacket and observe a single pulse in the time domain (Fig. 2d), corresponding to a broadband frequency spectrum (Fig. 2g). Figure 2h, i shows the dispersion curves of the mechanical travelling wave for different frequency detuning levels and different pump powers, respectively.

To provide further insight into the phenomena observed in Fig. 2, we have explored the effect of radiation force, which serves as the energy source to the mechanical mode. The strength of the radiation force driving the mechanical mode can be enhanced by increasing either the detuning of the pump frequency or the pump power. In Fig. 3a–c, we see that the localized pulse in the cnoidal wave regime is a slowly varying envelope of the oscillating optical signal induced by the periodic mechanical motion. By adjusting the frequency detuning and the pump power separately, we observe changes in the spectral features of the pulses, as shown in Fig. 3d–f and Fig. 3g–i, respectively. With an increase in the frequency detuning and pump power, the width of the pulse in the output field that is induced by the localized mechanical wavepacket decreases (Fig. 3d, g), while the period of the pulse increases (Fig. 3e, h). The peak value of the wavepacket is proportional to the input pump power (Fig. 3i) and also increases with the frequency detuning (Fig. 3f). When we increase the pump power or change the detuning Δ between the pump field and the cavity mode to Ω_m, more energy is transferred from the optical mode to the mechanical mode[47], leading to an enhancement of the optomechanically induced mechanical nonlinearity. In turn, the localized acoustic wave becomes narrower with a higher amplitude and a larger period. The cnoidal wave motion provides a more controllable way to generate mechanical frequency combs, in comparison to traditional approaches using wave-mixing processes[25,26]. Additionally, the localized wavepackets observed in our experiments are induced by the localized mechanical motion of the microtoroid, rather than optomechanical-induced localized photonic wavepacket (see our analysis in Supplementary Information section V).

The distinctive feature of our optomechanical solitons spanning a broad spectral window (as shown in Fig. 2g) indicates exciting opportunities for sensing applications. To show this, we exploit the optomechanical soliton to detect weak low-frequency vibrations of a cantilever tip actively excited by external electric pumping circuits (Fig. 4a). The

eigenfrequency of the mechanical cantilever tip is $\Omega_{tip} = 384.24$ kHz, which is far smaller than the eigenfrequency of the mechanical mode of the microtoroid. When the optomechanical resonator is in the periodic regime, it does not resonate with the low-frequency vibration of the tip. Consequently, we cannot observe the response of the optomechanical resonator to the vibrating cantilever tip (Fig. 4c). However, when the optomechanical resonator is in the soliton regime, with a wider power spectrum, more mechanical modes with different frequencies contribute to the response to the vibration of the cantilever tip. Although each mode gives a small contribution to the response to the tip vibration, which is far off resonance of the resonator, the collective contributions of all optomechanical modes are large enough to detect the low-frequency vibration of the cantilever tip (Fig. 4d). Figure 4b shows the detection efficiency increases with the width of the optomechanical soliton in the frequency domain. When the optomechanical soliton has a stronger localization in time domain, the width of the optomechanical soliton will increase. In this case, more modes of the optomechanical resonator will be involved, and therefore the enhancement will increase (Fig. 4b, inset).

In summary, we have reported the formation of a mechanical micro-soliton excited by light in an optomechanical microresonator. The stable mechanical soliton pulses result from two competing effects: (i) the dispersion of phonons induced by periodic modulation of the mechanical travelling wave owing to optomechanical interactions at the edge of the microtoroid; and (ii) optomechanically induced mechanical nonlinearity. We have also demonstrated that the shape of the mechanical soliton pulses can be controlled by tuning various system parameters, such as the pump power and the frequency detuning between the pump field and the cavity mode. The ability to localize phonons by optomechanically induced mechanical nonlinearity in nanostructures opens up new avenues for optomechanical applications. Cnoidal wave motion of the microtoroid resonator can be seen as a peculiar radio-frequency comb, and thus it may be useful for radio-frequency standards, clocks, astrocombs, and so on. The stable localized soliton pulse may be of great interest for sensing and transferring information in the radio-frequency regime using nanophotonic structures.

Online content

Any methods, additional references, Nature Research reporting summaries, source data, extended data, supplementary information, acknowledgements, peer review information; details of author contributions and competing interests; and statements of data and code availability are available at https://doi.org/10.1038/s41586-021-04012-1.

1. Holzwarth, R. et al. Optical frequency synthesizer for precision spectroscopy. *Phys. Rev. Lett.* **85**, 2264–2267 (2000).
2. Udem, T., Holzwarth, R. & Hänsch, T. W. Optical frequency metrology. *Nature* **416**, 233–237 (2002).
3. Haus, H. A. & Wong, W. S. Solitons in optical communications. *Rev. Mod. Phys.* **68**, 423–444 (1996).
4. Kippenberg, T. J., Holzwarth, R. & Diddams, S. A. Microresonator-based optical frequency combs. *Science* **332**, 555–559 (2011).
5. Herr, T. et al. Temporal solitons in optical microresonators. *Nat. Photon.* **8**, 145–152 (2014).
6. Kippenberg, T. J., Gaeta, A. L., Lipson, M. & Gorodetsky, M. L. Dissipative Kerr solitons in optical microresonators. *Science* **361**, eaan8083 (2018).
7. Brasch, V. et al. Photonic chip-based optical frequency comb using soliton Cherenkov radiation. *Science* **351**, 357–360 (2016).
8. Stern, B., Ji, X., Okawachi, Y., Gaeta, A. L. & Lipson, M. Battery-operated integrated frequency comb generator. *Nature* **562**, 401–405 (2018).
9. Suh, M.-G., Yang, Q.-F., Yang, K. Y., Yi, X. & Vahala, K. J. Microresonator soliton dual-comb spectroscopy. *Science* **354**, 600–603 (2016).
10. Yi, X., Yang, Q.-F., Yang, K. Y., Suh, M.-G. & Vahala, K. J. Soliton frequency comb at microwave rates in a high-Q silica microresonator. *Optica* **2**, 1078–1085 (2015).
11. Shao, L. et al. Microwave-to-optical conversion using lithium niobate thin-film acoustic resonators. *Optica* **6**, 1498–1505 (2019).
12. Forsch, M. et al. Microwave-to-optics conversion using a mechanical oscillator in its quantum ground state. *Nat. Phys.* **16**, 69–74 (2020).
13. Yamazaki, R. et al. Radio-frequency-to-optical conversion using acoustic and optical whispering-gallery modes. *Phys. Rev. A* **101**, 053839 (2020).
14. Aspelmeyer, M., Kippenberg, T. J. & Marquardt, F. Cavity optomechanics. *Rev. Mod. Phys.* **86**, 1391–1452 (2014).
15. Chan, J. et al. Laser cooling of a nanomechanical oscillator into its quantum ground state. *Nature* **478**, 89–92 (2011).
16. LIGO Scientific Collaboration and Virgo Collaboration. Observation of gravitational waves from a binary black hole merger. *Phys. Rev. Lett.* **116**, 061102 (2016).
17. Grudinin, I. S., Lee, H., Painter, O. & Vahala, K. J. Phonon laser action in a tunable two-level system. *Phys. Rev. Lett.* **104**, 083901 (2010).
18. Jing, H. et al. *PT*-symmetric phonon laser. *Phys. Rev. Lett.* **113**, 053604 (2014).
19. Zhang, J. et al. A phonon laser operating at an exceptional point. *Nat. Photon.* **12**, 479–484 (2018).
20. Carmon, T., Cross, M. C. & Vahala, K. J. Chaotic quivering of micron-scaled onchip resonators excited by centrifugal optical pressure. *Phys. Rev. Lett.* **98**, 167203 (2007).
21. Monifi, F. et al. Optomechanically induced stochastic resonance and chaos transfer between optical fields. *Nat. Photon.* **10**, 399–405 (2016).
22. Gan, J.-H., Xiong, H., Si, L.-G., Lü, X.-Y. & Wu, Y. Solitons in optomechanical arrays. *Opt. Lett.* **41**, 2676–2679 (2016).
23. Xiong, H., Gan, J. H. & Wu, Y. Kuznetsov–Ma soliton dynamics based on the mechanical effect of light. *Phys. Rev. Lett.* **119**, 153901 (2017).
24. Xiong, H. & Wu, Y. Optomechanical Akhmediev breathers. *Laser Photon. Rev.* **12**, 1700305 (2018).
25. Ganesan, A., Do, C. & Seshia, A. Phononic frequency comb via intrinsic three-wave mixing. *Phys. Rev. Lett.* **118**, 033903 (2017).
26. Butsch, A., Koehler, J. R., Noskov, R. E. & Russell, P. St. J. CW-pumped single-pass frequency comb generation by resonant optomechanical nonlinearity in dual-nanoweb fiber. *Optica* **1**, 158–163 (2014).
27. Savchenkov, A. A., Matsko, A. B., Ilchenko, V. S., Seidel, D. & Maleki, L. Surface acoustic wave opto-mechanical oscillator and frequency comb generator. *Opt. Lett.* **36**, 3338–3340 (2011).
28. Miri, M.-A., D'Aguanno, G. & Alù, A. Optomechanical frequency combs. *New J. Phys.* **20**, 043013 (2018).
29. Del'Haye, P. et al. Optical frequency comb generation from a monolithic microresonator. *Nature* **450**, 1214–1217 (2007).
30. Savchenkov, A. A. et al. Tunable optical frequency comb with a crystalline whispering gallery mode resonator. *Phys. Rev. Lett.* **101**, 093902 (2008).
31. Rueda, A., Sedlmeir, F., Kumari, M., Leuchs, G. & Schwefel, H. G. L. Resonant electro-optic frequency comb. *Nature* **568**, 378–381 (2019); correction 569, E11 (2019).
32. Zhang, M. et al. Broadband electro-optic frequency comb generation in a lithium niobate microring resonator. *Nature* **568**, 373–377 (2019).
33. Li, Q. et al. Stably accessing octave-spanning microresonator frequency combs in the soliton regime. *Optica* **4**, 193–203 (2017).
34. Cao, L. S., Qi, D. X., Peng, R. W., Wang, M. & Schmelcher, P. Phononic frequency combs through nonlinear resonances. *Phys. Rev. Lett.* **112**, 075505 (2014).
35. Czaplewski, D. A. et al. Bifurcation generated mechanical frequency comb. *Phys. Rev. Lett.* **121**, 244302 (2018).
36. Hao, H. Y. & Maris, H. J. Experiments with acoustic solitons in crystalline solids. *Phys. Rev. B* **64**, 064302 (2001).
37. Hereman, W. Shallow water waves and solitary waves. In *Encyclopedia of Complexity and Systems Science* (ed. Meyers, R. A.) 480 (Springer, 2009); https://doi.org/10.1007/978-0-387-30440-3_480.
38. Barland, S. et al. Temporal localized structures in optical resonators. *Adv. Phys. X* **2**, 496–517 (2017).
39. Lugiato, L., Prati, F. & Brambilla, M. *Nonlinear Optical Systems* (Cambridge Univ. Press, 2015).
40. Jang, J. K., Erkintalo, M., Murdoch, S. G. & Coen, S. Ultraweak long-range interactions of solitons observed over astronomical distances. *Nat. Photon.* **7**, 657–663 (2013).
41. Barland, S. et al. Cavity solitons as pixels in semiconductor microcavities. *Nature* **419**, 699–702 (2002).
42. Leo, F. et al. Temporal cavity solitons in one-dimensional Kerr media as bits in an all-optical buffer. *Nat. Photon.* **4**, 471–476 (2010).
43. Grelu, P. & Akhmediev, N. Dissipative solitons for mode-locked lasers. *Nat. Photon.* **6**, 84–92 (2012).
44. Korteweg, D. J. & de Vries, G. On the change of form of long waves advancing in a rectangular canal, and on a new type of long stationary waves. *Philos. Mag.* **39**, 422–443 (1895).
45. Boyd, J. P. The double cnoidal wave of the Korteweg–de Vries equation: an overview. *J. Math. Phys.* **25**, 3390–3401 (1984).
46. Nayanov, V. I. Surface acoustic cnoidal waves and solitons in a $LiNbO_3$-(SiO film) structure. *JETP Lett.* **44**, 314–317 (1986); translated from *Pis'ma Zh. Eksp. Teor. Fiz.* **44**, 245–247 (1986).
47. Fiore, V. et al. Storing optical information as a mechanical excitation in a silica optomechanical resonator. *Phys. Rev. Lett.* **107**, 133601 (2011).

Methods

Our system includes a high-Q whispering gallery mode optomechanical microtoroid resonator coupled to a tapered optical-fibre waveguide[19,48]. In our experiments, a tunable external-cavity laser diode in the 1,550-nm band was amplified by an erbium-doped fibre amplifier before it is coupled into a fibre connected to the tapered fibre waveguide. By changing the gap between the resonator and the tapered fibre, we could adjust the portion of the pump power coupled into the resonator. The output of the fibre-coupled resonator was fed into a photodetector that was connected to an oscilloscope, in order to monitor the time-domain behaviour of the transmission spectra, and also to an electrical spectrum analyser to obtain the power spectra.

Data availability

The datasets generated during and/or analysed in this study are available from the corresponding author upon reasonable request.

48. Carmon, T., Rokhsari, H., Yang, L., Kippenberg, T. J. & Vahala, K. J. Temporal behavior of radiation-pressure-induced vibrations of an optical microcavity phonon mode. *Phys. Rev. Lett.* **94**, 223902 (2005).

Acknowledgements The project is supported by the NSF grant number EFMA1641109 and ARO grant numbers W911NF1710189 and W911NF1210026. J.Z. is supported by the NSFC under grant numbers 61622306 and 11674194. Y.-x.L. is supported by the NSFC under grant number 61025022. Y.-x.L. and J.Z. are supported by the National Basic Research Program of China (973 Program) under grant number 2014CB921401, the Tsinghua University Initiative Scientific Research Program, and the Tsinghua National Laboratory for Information Science and Technology (TNList) Cross-discipline Foundation. L.L. is supported by the NSFC under grant number. 61925307. S.K. and A.A. are supported by the Office of Naval Research and the Air Force Office of Scientific Research.

Author contributions J.Z., B.P., F.M. and L.Y. conceived the idea. L.Y. designed the experiments. J.Z. performed the experiments and processed the data with the help of X.J., Y.L., P.Y. and L.L. J.Z. and S.K. provided theoretical analysis under the guidance of Y.-x.L. and A.A. J.Z. and L.Y. wrote the manuscript with contributions from all authors. L.Y. supervised the project.

Competing interests The authors declare no competing interests.

Additional information

Supplementary information The online version contains supplementary material available at https://doi.org/10.1038/s41586-021-04012-1.

Correspondence and requests for materials should be addressed to Lan Yang.

Peer review information *Nature* thanks the anonymous reviewers for their contribution to the peer review of this work. Peer reviewer reports are available.